Evaluation of Simultaneous Multisine Excitation of the Joined Wing SensorCraft Aeroelastic Wind Tunnel Model

Jennifer Heeg[1] and Eugene Morelli[2]
NASA Langley Research Center, Hampton, Virginia , 23681

Multiple mutually orthogonal signals comprise excitation data sets for aeroservoelastic system identification. A multisine signal is a sum of harmonic sinusoid components. A set of these signals is made orthogonal by distribution of the frequency content such that each signal contains unique frequencies. This research extends the range of application of an excitation method developed for stability and control flight testing to aeroservoelastic modeling from wind tunnel testing. Wind tunnel data for the Joined Wing SensorCraft model validates this method, demonstrating that these signals applied simultaneously reproduce the frequency response estimates achieved from one-at-a-time excitation.

Nomenclature

Abbreviations

AEI	Aerodynamic Efficiency Improvement	DFT	Discrete Fourier Transform
ANOVA	Analysis of Variance	FWI	Forward Wing Inboard
ACC	Accelerometer	FWM	Forward Wing Middle
AWI	Aft Wing Inboard	FWO	Forward Wing Outboard
AWM	Aft Wing Middle	JWS	Joined Wing SensorCraft
AWO	Aft Wing Outboard	SG	Strain Gauge
CPE	Controller Performance Evaluation	TDT	Transonic Dynamics Tunnel

Symbols

dfstp	=	Multisine signal frequency spacing parameter	A_i	=	Amplitude, ($\sqrt{Power}$) , of ith sine wave component
f	=	Frequency, Hz	C	=	Command
f_i	=	Ith frequency contained in the multisine signals	G	=	Open loop plant transfer matrix
f_{max}	=	Maximum frequency contained in the generated multisine signals, Hz	H	=	Control law transfer matrix
$\widetilde{f_{max}}$	=	Maximum specified frequency for the multisine signals to contain, Hz	N	=	Total number of time samples
$\widetilde{f_{min}}$	=	Minimum specified frequency for the multisine signals to contain, Hz	Ni	=	Number of sinusoidal components comprising a multisine signal
f_0	=	Fundamental frequency of a time history, = 1/T, Hz	Ns	=	Sample size, number of experiments
j	=	$\sqrt{-1}$	T	=	Length of time history, sec
k	=	Fourier domain index	U	=	Excitation
n	=	Time sample number	X	=	Control law output
nfft	=	Number of samples in a Fourier Transform computation	Xuc	=	Controller output transfer matrix
ni	=	Number of orthogonal multisine signals in a set	$\tilde{X}[k]$	=	The kth Fourier coefficient

[1] Senior Research Engineer, Aeroelasticity Branch, Mail Stop 340, Senior Member AIAA.
[2] Research Engineer, Dynamic Systems and Control Branch, Mail Stop 308, Associate Fellow AIAA.

samp	=	Sample rate of acquired data
$t_{(\alpha/2,N-1)}$	=	upper critical value of Student's t-distirubtion with N-1 degrees of freedom, and a confidence coefficient of 1-α.
$u_i(t)$	=	The ith multisine signal
$\breve{u}_i(t)$	=	The ith sinusoidal component time history
$\tilde{x}$ [n]	=	A sample of the time history signal

Subscripts

sym	=	Symmetrized, (right + left)/2
left	=	Located on the left wing
right	=	Located on the right wing

Y	=	Sensor response
Yuc	=	Plant output transfer matrix
Δf	=	Frequency spacing
ε	=	strain
μ	=	Mean value estimate
φ_i	=	Phase offset of the ith sine wave component
σ	=	Standard deviation estimate
ω	=	Frequency, radians/sec

Introduction

Vehicle systems for modern aircraft incorporate an increasing number of control surfaces and devices, allowing the design to have enhanced control capability and robustness to failures. Control of the aeroelastic behavior is one area where multiple control effectors can be beneficial, by distributing control authority to where it is most effective. As the number of available control effectors increases, assessing their individual influences becomes more time consuming and challenging. The current study evaluates a promising methodology for efficient identification of aeroservoelastic systems with large numbers of control effectors.

A method for optimal multiple input design for evaluating stability and control parameters has been developed and applied in flight[1]. This method involves superposition of harmonic sinusoids with frequency content in the range of the dynamics of interest and phase optimization to minimize peak-to-peak amplitudes. The approach is of interest here because it can be used to generate excitation signals that are simultaneously applied to multiple control effectors and produce responses which are separable according to the contribution of the individual control effectors. This approach is accomplished by determining the Fourier transform frequency content that is resolvable within the excitation time length and distributing that frequency content among the control effectors. Multiple excitation signals which are orthogonal in both the time and frequency domains can be generated based on the frequency parsing of harmonic sinusoids, which may then be applied simultaneously to the set of multiple control effectors.

The work presented here endeavors to extend the range of application of this established excitation methodology. Application to an aeroelastic problem requires a significantly larger frequency range for the excitation than that typically required for stability and control parameters estimation. The increase in frequency range is not readily traded for decreasing the resolution of the frequency range because resolving aeroelastic modal characteristics often demands more dense frequency spacing than steady or quasi-steady aerodynamic quantities. This demand leads to a significant increase in the number of sinusoidal harmonics which are required to comprise a single multisine excitation.

These concepts were investigated through a wind tunnel experiment using the Joined Wing SensorCraft (JWS) model. Results are presented for the model in two configurations: one without control laws active and one with rigid body trim control loops closed. The process and results for extracting the open loop aeroelastic system frequency response estimate from closed loop data are also presented. In performing system identification experiments and data reduction, numerous decisions must be made. The influences of the following choices are discussed: data processing parameters for the Fourier analysis, excitation signal amplitude, and excitation signal frequency content.

I. Wind Tunnel Model and Testing

The Joined Wing SensorCraft (JWS) project is one element in the Aerodynamic Efficiency Improvement (AEI) program led by the Air Force Research Laboratory[2]. The Boeing Aircraft Company developed the JWS configuration to address the AEI mission and requirements[3,4] ; the wind tunnel model was designed, fabricated[5,6] and tested[7,8] by a collaborative team from the United States Air Force, the Boeing Company, NextGen Aeronautics, Millennium Dynamics and NASA.

The JWS is a unique configuration with two sets of non-co-planar high aspect ratio wings. The forward wings sweep aft, and the aft wings sweep forward; the aft wings join the forward wings near the ¾ span. This configuration is highly flexible, requiring multiple simultaneous control strategies.

The JWS was tested in the NASA Langley Transonic Dynamics Tunnel (TDT)[9] during three test periods. The first test, performed with the model mounted on an aft sting, Figure 1, allowed model and system checkout, procedure evaluations and preliminary system identification. The primary research was conducted during follow-on tests with the model free to travel vertically on a beam and rotate about its pitch axis, Figure 2.

The primary research objectives of the JWS tests were to demonstrate controlled flight with reduced static stability, measure the stability margins in flight, and alleviate gust loads in the frequency range of the first two symmetric aeroelastic modes. The test objectives did not require extensive investigation at multiple test conditions; all test data contained in the current report was acquired at a single tunnel condition using R134a as a test medium: Mach 0.22, dynamic pressure 51 psf.

Figure 1. JWS model in TDT in aft sting mount test configuration, Test 606

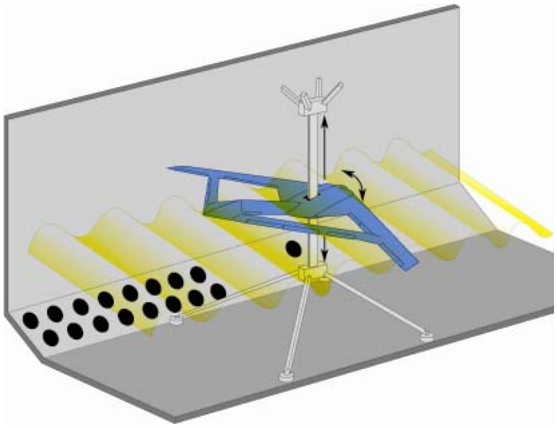

Figure 2. Illustration of JWS model in TDT on mount system allowing pitch and plunge freedom, Tests 613 and 614

Addressing the vehicle and structural controls objectives resulted in a design with 13 independent control surfaces. The planview, Figure 3, shows the six forward wing control surfaces in various shades of green, and the six aft wing control surfaces in various shades of red. For the research reported here, the control surfaces were actuated symmetrically, in pairs. Additionally, there is a rudder not visible from the presented viewpoint, located on the aft boom connecting the fuselage with the aft wing root structure. The rudder was not used in any of the research in this report. Details of the hydraulic actuation system are provided in reference 8.

The sensor information which will be highlighted in the current work comes from bending strain gauges and vertically-oriented accelerometers located in the wings, shown in Figure 3.

The six aft wing control surfaces were utilized in the trim control laws that were active while obtaining the system identification data presented in this report. The sensors utilized in the trim controller were those corresponding to rigid body motion, rather than the aeroelastically-responsive sensors which are emphasized in the current study and utilized in the gust load alleviation control task. Reference 8 contains details of the control laws, their implementation and results.

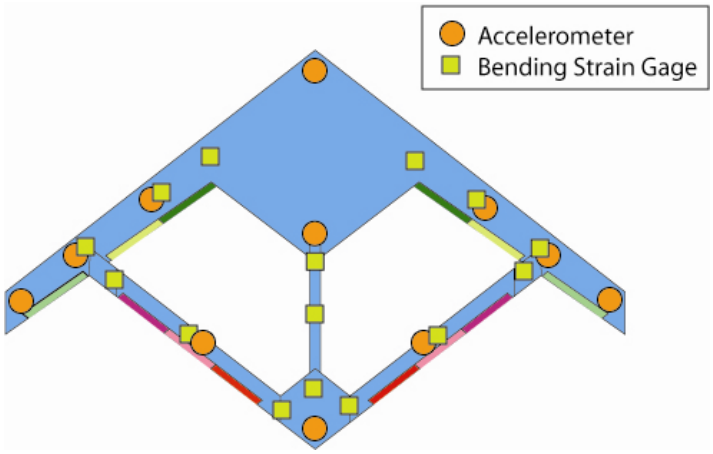

Figure 3. Layout of Joined Wing SensorCraft wind tunnel model, with primary sensors and control surfaces for system identification studies

The multisine excitation implementation required the development of an auxiliary system. Rather than substantially modifying the primary control computer software, a Labview interface was developed for use with National Instruments boards. The system was developed such that arbitrary time histories could be output simultaneously to 16 channels in real time. The conceptual block diagram of the system and its interaction with existing JWS systems is shown in Figure 4. Details of the JWS Control Computer and Signal Generator 1 are provided in reference 8.

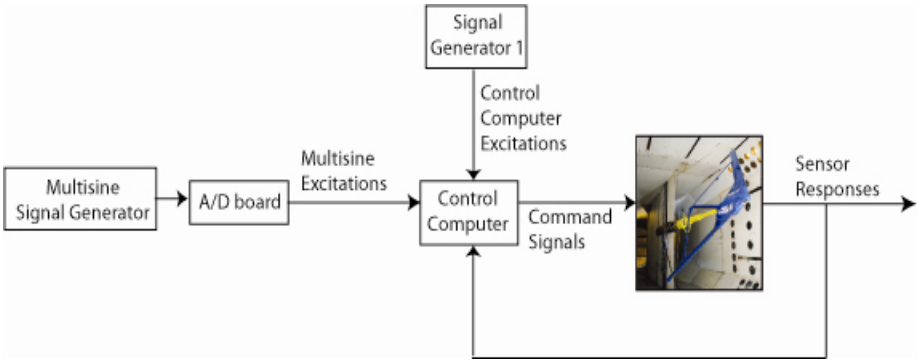

Figure 4. Conceptual Block Diagram of Joined Wing SensorCraft excitation using external signals

II. Multisine Excitation Design

Aeroelastic properties are often viewed through the lens of frequency domain characterization. This perspective is useful when considering the possibilities offered by the multisine excitations developed in reference 1. A multisine signal is composed by adding sine wave time histories. Each multisine signal is a sum of harmonic sinusoid components with unique frequencies. Since each multisine signal contains harmonics with frequencies that no other multisine signal has, all of the multisine signals are mutually orthogonal in both the time and frequency domains. The frequency content of each multisine signal and the power at each frequency are chosen so that applying each signal to a different input of the system can adequately excite the system dynamics over the frequency range of interest. Sinusoidal time histories are specified by the following parameters: frequency, phase, amplitude and time length. Each of these is utilized in designing sets of multisine signals such that they excite the system over the frequency range of interest, also achieving a specified frequency resolution.

The frequencies used in constructing the multisine component sine waves, f_i, are calculated as integer multiples of the fundamental frequency, f_0, of the excitation time length specified. These frequencies are identical to the frequencies used in computing the discrete Fourier transform (DFT) of a signal of this same time length.

$$f_0 = 1/T$$
$$f_i = i * f_0$$

The frequencies of the sine waves that are used are determined based on specified approximate minimum and maximum frequencies- integer multiples of the fundamental frequency that bracket the specified frequency range are

retained. Additionally, a frequency spacing parameter, dfstp, can be specified. The frequencies retained in generating the signals are given in Equation 1. The maximum frequency is calculated using Equation 2. The floor function used in Equation 1 rounds the quantity downward, to the next lowest whole number; the ceiling function used in Equation 2 rounds the quantity upward, to the next highest whole number.

$$f_i = f_0 * \left\{ floor\left(\frac{\widetilde{f_{min}}}{f_0}\right) + (i-1) * dfstp \right\} \quad \text{Equation 1}$$

$$f_{max} = f_0 * \left\{ ceil\left(\frac{\widetilde{f_{max}}}{f_0}\right) \right\} \quad \text{Equation 2}$$

In reference 1, the phase angles of individual sinusoidal components were chosen by an optimization technique to minimize peak-to-peak amplitude in the multisine signal. The large number of components required to comprise excitations to aeroelastic systems makes that optimization very time-consuming. For the current research, the phase of each sine wave component was randomly set to a value between $-\pi$ and π. This leads to several issues which are discussed subsequently.

The relative amplitude of each sine wave component was determined in three ways during this test. Uniform power, logarithmic power as a function of frequency and highly tailored power distributions were each utilized. These distributions are similar to employing a linear sine sweep, a logarithmic sine sweep and bandpass frequency range sine sweeps. The overall amplitude factor for a multisine signal was scaled such that the power of the signal, summed over all of the frequencies within the signal equaled 1. The power for each sinusoidal component is the square of that component's amplitude. For the case of a uniform distribution over a frequency range with nf discrete frequencies, this means that each component's amplitude is $1/\sqrt{nf}$.

The equation for generating each sine wave component is given by Equation 3.

$$\tilde{u}_i(t) = A_i * \sin(2\pi f_i t + \varphi_i) \quad \text{Equation 3}$$

The number of multisine signals, ni, in an orthogonal set is user-specified, and determines the spacing of the frequency content. In the JWS testing, as many as 13 orthogonal multisine signals were required. In this case, the first multisine signal had content at the 1st, 14th, 28th, etc frequencies as calculated in Equation 1. The multisine signals are created by summing the component sine waves, Equation 4.

$$u_j(t) = \sum_{i=j}^{Ni} \tilde{u}_{((i-1)*ni+j)}(t) \quad \text{Equation 4}$$

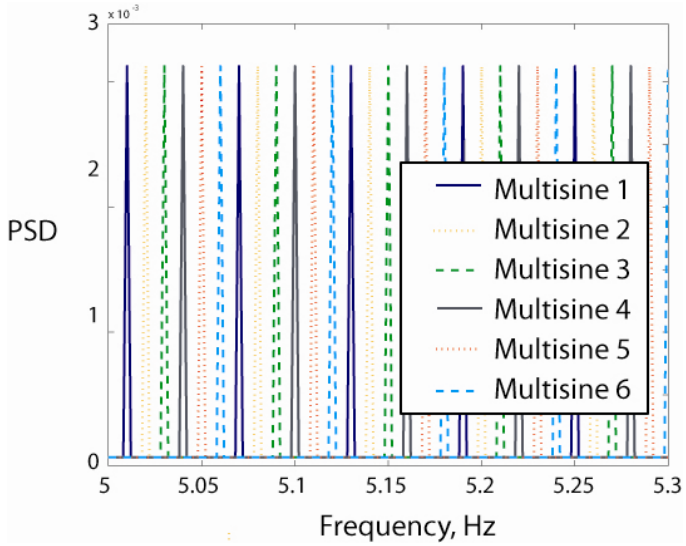

Figure 5. Multisine signal frequency content example; 6 orthogonal signals; fmin = 0.1 Hz, fmax = 10 Hz, dfstp = 1, T=100 sec, samp=200 samples/sec

Much of the data acquired during the JWS test used 6 orthogonal multisine excitations with content from 0.1 Hz to 10 Hz, with a time length of 100 seconds, using all of the available Fourier analysis frequencies in that range (dfstp = 1). The specified component sine waves were usually discretized at 200 samples/second.

Each orthogonal time history contains frequency content at unique frequencies, calculated using Equation 1, and parceled out as shown in Figure 5. The example parameters produce six time histories, two of which are shown in Figure 6. The plot in Figure 5 shows only 5 frequencies contained in each of the orthogonal multisine time histories; for this example, each multisine signal is a composite of 165 sine wave components, each with random phase assigned. The frequency spacing within each signal is 0.06 Hz, corresponding to frequency spacing of 6 times the fundamental frequency of a 100 second time history.

$$\Delta f = ni * f_0$$

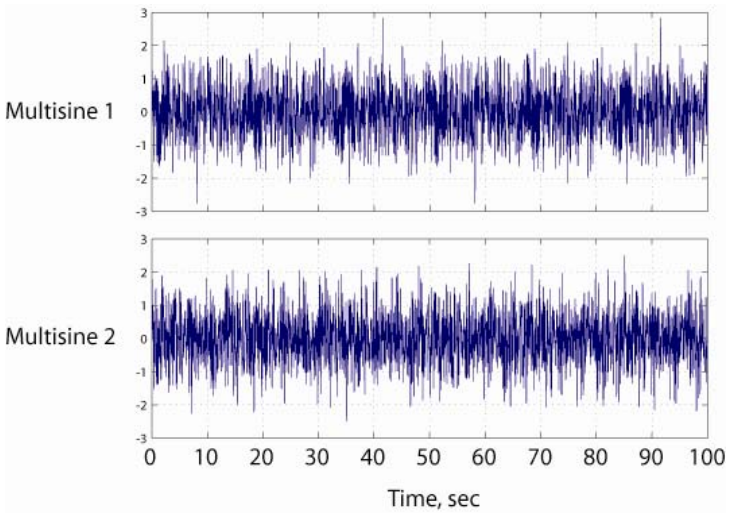

Figure 6. Example multisine signals with realistic test parameters; Full set contains 6 orthogonal multisine signals with content from 0.1 Hz to 10 Hz

There are consequences to the random method of assigning phase angles in constructing the multisine signals, rather than determining the phase angles by optimization. Utilizing optimization would allow the maximum excitation content over the frequency range desired without exceeding the control surface limits. The outcome of the optimization effort would reshape all of the multisine signals within an orthogonal set. Without the optimization, some of the resulting signals contain large peaks where multiple sine waves are near their maximum values simultaneously. Applying these signals to excite the model then requires that the overall amplitude factor decreased to remain within the control surface command limits, thus reducing the excitation level. This limitation was partially overcome by early examination of the orthogonal signal set. When a set of signal design parameters resulted in time histories with large peaks, the design process was repeated by selecting a new set of random phase angles until the random phase angle selection produced an acceptable set of orthogonal signals. No signal design had to be repeated more than once to obtain an acceptable set.

III. Test Results

This section presents frequency response estimation results. The estimates are computed through Fourier transform analysis of measured time histories using standard techniques[10] to characterize open loop and closed loop system responses.

Data for the model clamped to the mount system is presented first. This is the only test configuration where data is available for an open loop system, i.e. without a control law active. No closed loop data is available for the model in this configuration. Data is next presented for the model flying on the support system, controlled with a low-frequency trim control law. The primary test objective was gust load alleviation of the model while it was free to plunge and pitch. Thus, most of the system identification data obtained and analyzed corresponds to trimmed flight, which is necessarily closed loop. The process for producing the open loop results and the closed loop results, respectively, for the two cases above are straight-forward and identical. Frequency response estimates of sensor measurements of output responses due to control surface inputs are evaluated through the ratio of the cross-spectrum and auto-spectrum estimates for the measured output and input signals.

It is also desired to demonstrate open loop system extraction using closed loop data and identify additional errors or uncertainties associated with this process. There is, however, a disconnect in the available data sets. One is the open loop clamped configuration; the other is the closed loop flying configuration. Using the available closed loop data, the method of return difference matrices[11,12] was applied to estimate the open loop flying system characteristics. However, there is no corresponding "truth" open loop data available for comparison. Thus, quantification of errors and assignment to processing sources cannot be accomplished with the current data set.

Analysis results of multisine signals presented in this section were all generated using identical sets of Fourier analysis parameters: a block size of 4096 points was utilized to analyze time histories of 100 seconds of data. All data was acquired at 500 samples/sec; 95% overlap of blocks was utilized. Rectangular windowing was applied to the data, and only the portions of the time histories with the excitations applied were included in the analysis. All signals were detrended prior to Fourier transformation.

Comparison data sets generated using sine sweeps, are also presented in this paper. These data sets were analyzed with parameters identical to the above specification, except that the excitation lengths varied: 60, 65 and 100 seconds. This difference does not modify the analysis frequencies, as the analysis block size is significantly shorter than the time record lengths. The shorter time record lengths, however, result in fewer averages for the sine sweep data than for the multisine data.

Although data is available for varying center of gravity positions, all data shown here will be for the forward-most location, 5% positive static margin. Only symmetric excitation data will be presented here, where a set of control surfaces- left wing and right wing pairings- are identically deflected. Deflecting any pair of control surfaces on the model produces responses at each of the strain gauges and accelerometers, however, the data to be shown here will only show the proximal strain or acceleration for a given control surface deflection, except where specifically noted. The forward outboard control surfaces showed the greatest control authority throughout the JWS testing, producing the cleanest frequency responses because of superior signal-to-noise ratios.

A. Open loop clamped configuration results

One of the postulations for this investigation was that aeroelastic frequency responses due to individual control surfaces can be obtained by simultaneous multisine actuation of all control surfaces. Applying a sine sweep excitation to a single set of control surfaces, applying a multisine signal to a single set of control surfaces, and applying a set of orthogonal multisine signals to all control surfaces produce frequency response results which are similar in character and reasonably close in magnitude and phase. There is a substantial difference between this triad of results and the pair of results generated by actuating all surfaces simultaneously with a sine sweep or by applying an identical multisine signal to all of the surfaces.

Frequency response results of strain (FWO location) due to FWO deflection are shown as a function of frequency in Figure 7. Five data sets are shown on this plot: two utilize only the FWO control surfaces; three utilize all control surfaces simultaneously.

The first data set (solid red) was produced by applying a sine sweep to only the FWO control surfaces. The equivalent multisine data (solid cyan) was produced by applying a single multisine signal to the FWO control surfaces. The frequency content and the energy imparted over the frequency range of these signals were roughly equivalent and the results expectedly similar. The third set of data (black dot-dash) was produced by applying 6 orthogonal multisine signals simultaneously, one orthogonal signal to each of the six pairs of control surfaces. Because the signals are orthogonal, the resulting frequency domain characterization for each of the control pairs is also orthogonal. The result is that the identified frequency response for the FWO control surfaces is not polluted by the actuation of the other pairs of control surfaces. In the plot, the black dot-dash line agrees well with the solid red and solid cyan lines. The aeroelastic frequency responses due to individual control surfaces can be obtained by simultaneous multisine actuation of all control surfaces. Applying a sine sweep excitation to a single set of control surfaces, applying a multisine signal to a single set of control surfaces, and applying a set of orthogonal multisine signals to all control surfaces produce the frequency response results which are qualitatively similar. Quantitative assessment of the variation among these data sets was not performed due to the limited number of data sets for the clamped configuration.

The remaining two sets of data in the figure correspond to cases where simultaneous identical signals are applied to all control surfaces; sine sweep (red dashed) and multisine (orange dashed) signals produce results similar to each other, but corresponding to the case when all surfaces are utilized as a single control surface. Although not shown in the plot, these results compare well to the case where all frequency responses are generated due to each control surface pair and the results summed. Again not shown in the plot, the same results are produced by individually actuating each control surface pair and adding the time histories of the responses together. This creates a frequency response that treats all control surfaces as a single control effector.

Most pertinent to the current work, the deviation of these two data sets from the first three illustrate that Fourier analysis cannot accomplish the separation of frequency responses when identical excitations are applied to the various control effectors.

The orthogonal multisine signal results will differ from the individual actuation results when there are physical control surface interference effects. Examples of physical interference effects include the aerodynamic effect of deflecting one control surface on the flow field experienced by the surrounding control surfaces, and the influence of deflecting one control surface on the surrounding structure which influences the geometry and loading of the other control surfaces. The physical interference component will also be present for the cases when all surfaces are actuated simultaneously using other types of signals. These other simultaneous actuation scenarios, however, do not allow for separate identification of the portion of the sensor response due particularly to a specific control surface.

Under ideal repeatability and data handling conditions, the small difference between the orthogonal multisine excitation and either of the individual excitation responses would be assignable to control surface interference effects. The large difference between the two all-actuated frequency responses and the first three data sets incorporates the control surface interference effects, but the difference is primarily produced by the effect of the sensor responding to identical excitations sent to the other control surfaces, which is the equivalent of estimating the frequency response for a larger effective control surface consisting of all the control surfaces that are moved together.

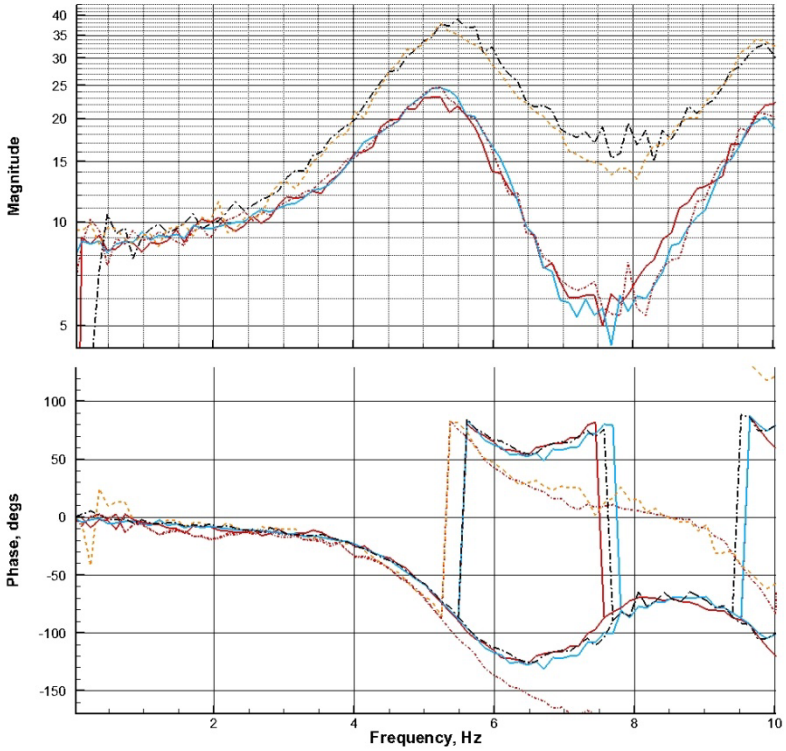

	Number of Signals	Signal Type	Surface Pairs Used
	1	Sine sweep	1
	1	Multisine	1
	6	Multisine	6
	1	Sine sweep	6
	1	Multisine	6

Figure 7. Frequency response of Forward wing outboard strain gauge due to forward wing outboard surface command; Clamped configuration, open loop system

Analyses identical to those described above were performed for each of the sensors on the model, relative to each of the actuation pairs. These additional frequency response comparisons are not shown here; the comparisons are similar to those of the closed loop free body configuration which will be shown in detail in the following section

B. Closed loop trimmed flight configuration results

The trimmed flight configuration was the primary JWS test configuration. As such, there are many more sets of data acquired when the model is flying rather than when clamped. Frequency response estimates for this system were obtained and processed identically to those of the clamped configuration. For this data, however, there is always a trim control law active. Thus, the system identified in this section is different from the previous system- it has a different boundary condition, and it is a closed loop controlled system. Figure 8 shows a comparison of frequency response estimates for the open loop clamped configuration and the closed loop trimmed flying

configuration. The data shown is frequency response estimate magnitudes produced using sine sweep excitation to the forward wing outboard control surface pair. The altered boundary condition is primarily responsible for the observed difference in the modal frequencies. The clamped model's lowest frequency aeroelastic modes, shown by peaks on the graph, occur near 5.2 and 10.1 Hz, while the flying model frequencies are lower, near 4.9 and 7.4 Hz. The trim control law is primarily responsible for the reshaping of the low-frequency characteristics, observed as reduced amplitude below 2 Hz for the closed loop flying system.

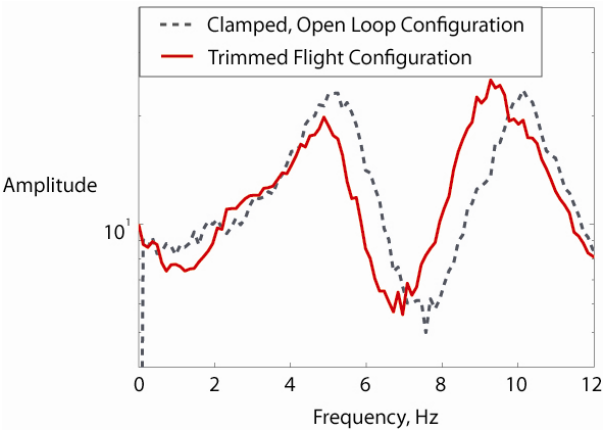

Figure 8. Comparison of clamped open loop configuration with trimmed flight configuration (SGFWO/FWO)

The strain and acceleration frequency response estimates for the closed loop system are shown in Figure 9 and Figure 10. Multiple data sets are shown in each plot for the sine sweep excitations and the multisine excitations- for this configuration, repeat data sets were obtained at various points during testing. Figure 9 shows the frequency response estimates of the strains due to control surface deflections. Each subplot shows the symmetrized response of the gauges closest to the respective control surface pair. Symmetrization of the responses was performed in the time domain, employing Equation 5.

$$\varepsilon_{sym} = \frac{(\varepsilon_{right} + \varepsilon_{left})}{2} \qquad \text{Equation 5}$$

Sine sweep excitations applied to a single control surface pair generates frequency response estimates shown by red lines; three sine sweep data sets are shown in each of the subplots. Multisine excitations applied to a single control surface pair result in the cyan lines; only 1 of these cases is shown in the subplots. Orthogonal multisine excitations are shown by the black lines; three orthogonal multisine data sets are shown in each subplot.

The accelerometer frequency responses, shown in Figure 10 are generally cleaner than the strain responses. The data sets shown follow the same conventions as the previous figure.

All comparisons show good qualitative agreement among the three excitation methods. There are, however, some discrepancies among the three data sets.

	Number of Signals	Signal Type	Surface Pairs Used
———	1	Sine sweep	1
- - -	1	Sine sweep	1
·····	1	Sine sweep	1
———	1	Multisine	1
- - -	1	Multisine	1
———	6	Multisine	6
- - -	6	Multisine	6

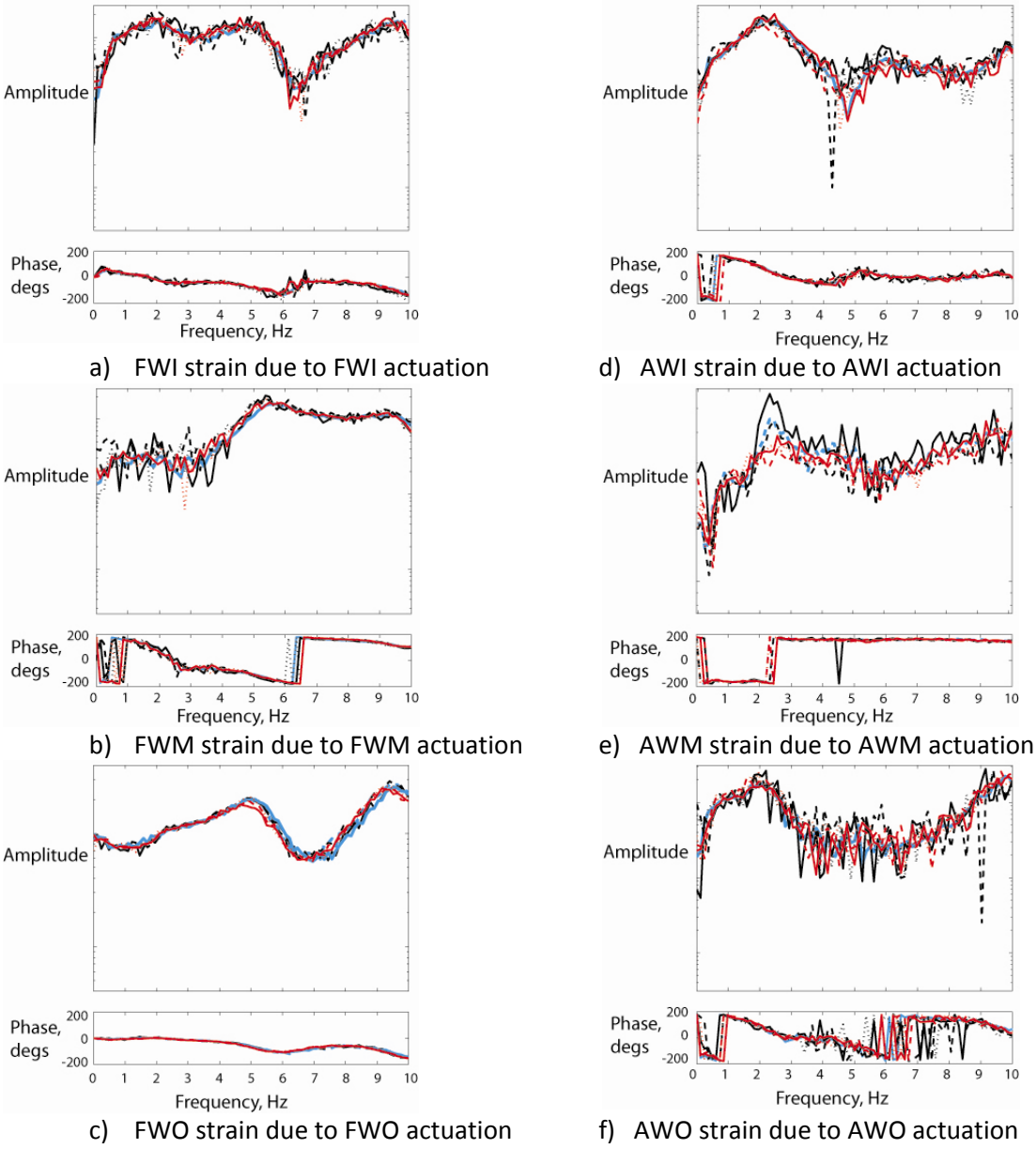

Figure 9. Symmetrized strain frequency responses due to co-located control surface pair actuation; Trimmed flying configuration, closed loop

	Number of Signals	Signal Type	Surface Pairs Used
———	1	Sine sweep	1
- - -	1	Sine sweep	1
·····	1	Sine sweep	1
———	1	Multisine	1
- - -	1	Multisine	1
———	6	Multisine	6
- - -	6	Multisine	6

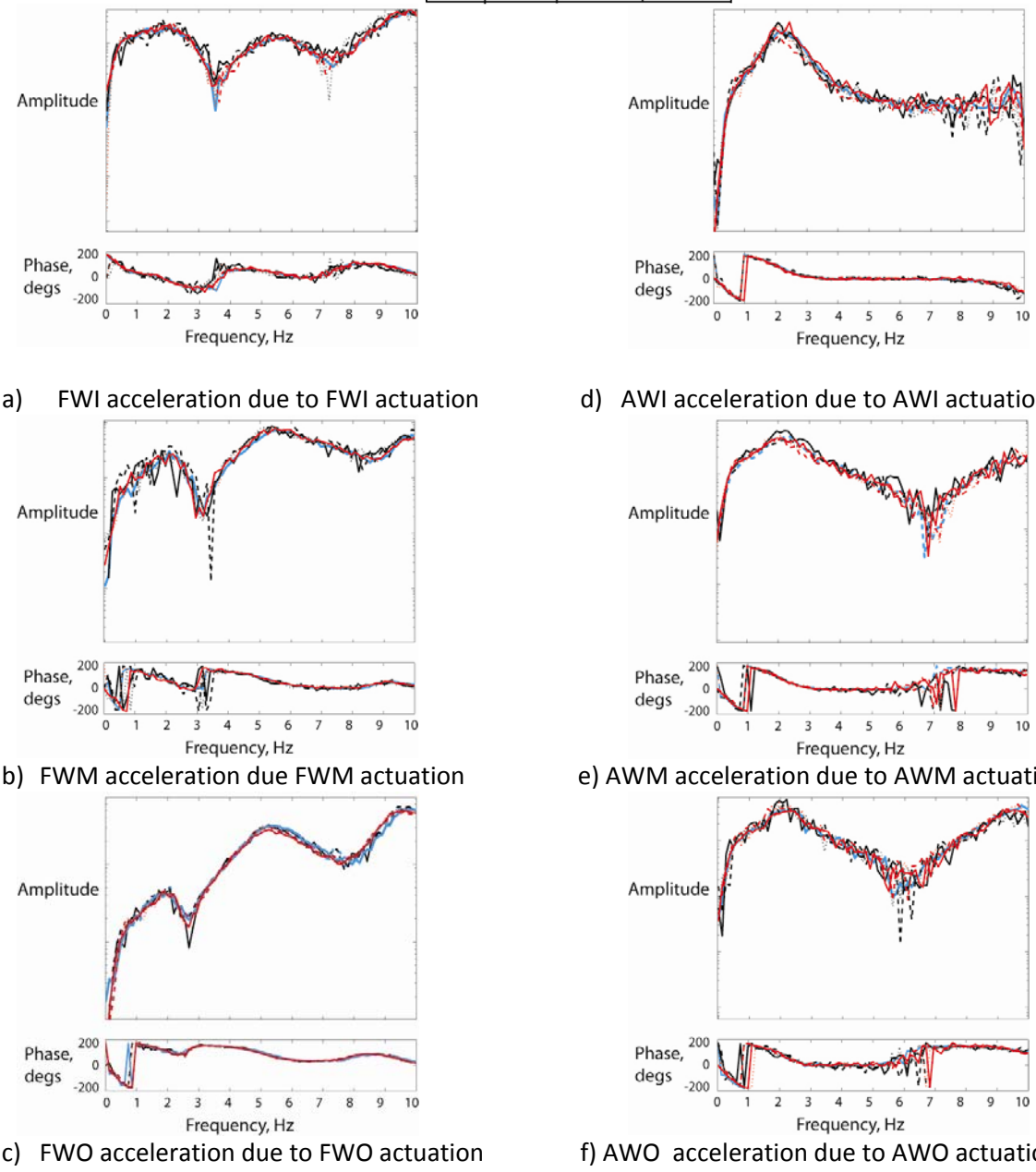

a) FWI acceleration due to FWI actuation

d) AWI acceleration due to AWI actuation

b) FWM acceleration due FWM actuation

e) AWM acceleration due to AWM actuation

c) FWO acceleration due to FWO actuation

f) AWO acceleration due to AWO actuation

Figure 10. Symmetrized accelerometer frequency responses due to co-located control surface pair actuation; Trimmed flying configuration, closed loop

The comparison between single surface actuation using sine sweeps and multisine signals appear to show as much or more variation than the comparison between single surface multisine and all-surface orthogonal multisine results. These results are evaluated quantitatively in a subsequent section of this paper.

C. Open loop flight configuration extracted results

Commercial and military aircraft and free-flying wind tunnel models usually operate with control laws active- that is, with the controller loop closed. It is often desirable to characterize the vehicle or model without the control law effects- that is, identify the open loop system. We now present the process applied and results achieved for extracting the open loop system from closed loop system excitation. Open loop plant extraction using the return difference matrices is a subset of controller performance evaluation (CPE) methods described in references 11 and 12. Previous applications of CPE methodology required actuation of one control effector at a time and combining these separate data sets. Using the multisine excitation method allows calculation of all required components using measurements from a single experiment.

Calculation via the return difference matrices is necessitated by non-orthogonalities introduced by the control law feedback. In applying multisine excitations, only the actual excitations are orthogonal- not the feedback signals. The CPE method, detailed in the cited literature produces the equation for computing the open loop plant from the closed loop data.

$$\boldsymbol{G} = \left[\left(\mathbf{1} - \boldsymbol{X}_{\boldsymbol{uc}}^{\boldsymbol{T}}\right)^{-\mathbf{1}} \boldsymbol{Y}_{\boldsymbol{uc}}^{\boldsymbol{T}}\right]^{\boldsymbol{T}} \qquad \text{Equation 6}$$

The CPE method accounts for the presence of the feedback loop, while a direct method makes the assumption that the inputs to the open loop system are orthogonal to each other. Signal naming conventions are illustrated in the block diagram shown in Figure 11. The *excitations* which are used are orthogonal to the precision of the discretization and recording process, but the open loop system inputs are nonorthogonal due to those effects *plus* the effects of the control law feedback. The control law feedback signals contain components which are co-directional with each input excitation. That is, the control law feedback signals can be broken into their orthogonal components, assuming that the control law is linear. Another way of saying this is that the control law output signals have components which are correlated to each of the excitations present. The CPE method works by decomposing the sensor signals and the control law output signals into the orthogonal components produced by each of the orthogonal excitations.

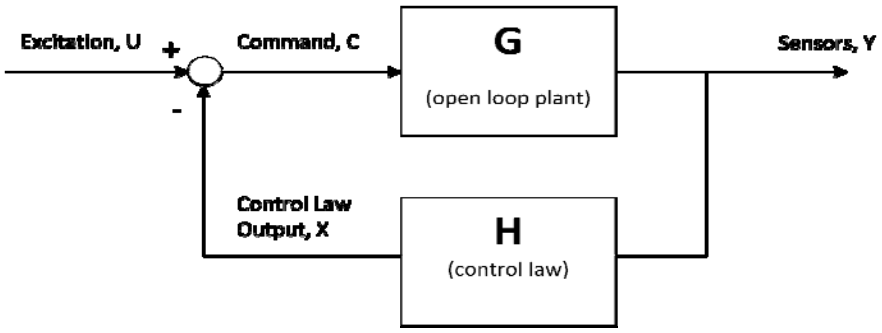

Figure 11. Closed loop system block diagram with signal names and sign conventions

A sample result of applying the CPE method is shown in Figure 12. The results are compared with the closed loop system data that was used to extract the open loop information. There is little difference evident between the open loop and closed loop systems in the aeroelastic range because the trim control law effects are concentrated at frequency below the first aeroelastic mode. These results serve as a demonstration of the CPE method using the simultaneous multisine excitations. Because data from the open loop test configuration is not available, these results should not be viewed as conclusively demonstrating the process.

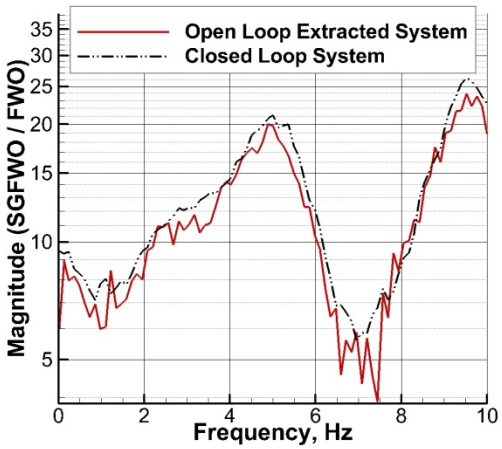

Figure 12. Extracted open loop system frequency response estimate from closed loop data

IV. Influence of data analysis and excitation parameters

A. Fourier analysis parameter effects

The results shown in this paper come from Fourier analysis. The choices made in performing the data reduction are next explored. The relationship between analysis frequency spacing and excitation frequency spacing is of particular and practical importance. Successful design of the excitation signals must incorporate consideration of the analysis parameters.

In the data reduction performed, the discrete Fourier transform (DFT) is heavily relied upon. From Oppenheim and Schafer[13], the DFT is defined by Equation 7.

$$\tilde{X}[k] = \sum_{n=0}^{N-1} \tilde{x}\,[n] e^{-j\left(\frac{2\pi}{N}\right)kn} \qquad \text{Equation 7}$$

Each multi-sine excitation contains sinusoidal content at a specified number of frequencies over a specified frequency range. The spacing of the analysis frequencies should be greater than that of the excitation, Equation 8. The analysis and excitation frequency spacing are separately controlled; calculations of these quantities utilize Equation 9Equation 10.

$$\Delta f_{analysis} \geq \Delta f_{excitation} \qquad \text{Equation 8}$$

$$\Delta f_{analysis}(Hz) = \frac{samp}{nfft} \qquad \text{Equation 9}$$

$$\Delta f_{excitation} = \left(\frac{1}{T}\right) * dfstp * ni \qquad \text{Equation 10}$$

Analyzing the data with more densely populated frequency spacing results in frequency response calculations that may at first glance resemble noise. Buried within that "noise" is a good representation of the frequency response, but it must be carefully extracted. The following example illustrates these points.

Figure 13 shows the magnitude of the frequency response estimate of the forward wing outboard strain gauge response due to forward wing outboard control surface excitation. In this example, the excitation was generated using frequency spacing of 0.49 Hz. The Fourier analysis was performed with an analysis block size of 2^13, or 8192, points. The sample rate of the data acquisition was 500 Hz. Using Equation 9 shows that the analysis frequency spacing for this case is thus 0.061 Hz, violating the criterion set out in Equation 2. The consequence is the very scattered appearance of the frequency response.

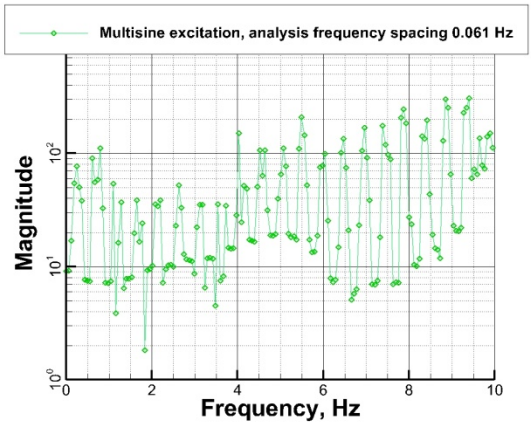

Figure 13. Frequency response estimate using Fourier analysis frequency spacing of 0.061 Hz and multisine excitation frequency spacing of 0.49 Hz

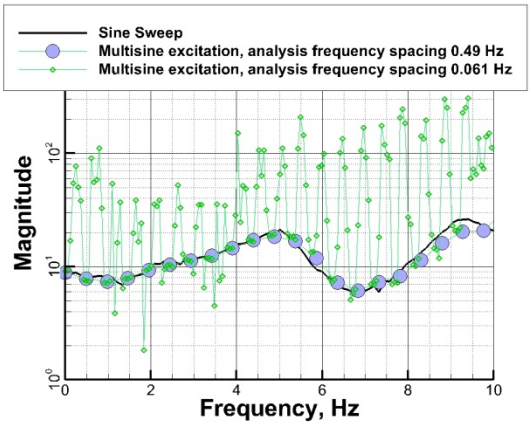

Figure 14. Effect of Fourier analysis frequency spacing

Applying the frequency spacing requirement, the minimum spacing requirement is achieved by using a Fourier analysis block size of 2^10 points, 1024. The frequency response that results from this analysis is shown in Figure 14. The results from analysis of sine sweep data and the previous Fourier analysis are shown for comparison. Note that the frequency response points could have been determined by proper down-selection of the points calculated using the denser population; a subset of points from the original frequency response match those of the frequency response computed with the proper analysis frequency density.

B. Excitation amplitude effects- signal to noise ratio

One non-ideal condition in flight or a wind tunnel test is the presence of turbulence. This condition is a source of unspecified, uncontrolled and unknown excitation which will affect the model response. Increasing the amplitude of the applied excitation decreases the relative influence of the turbulence, resulting in increasing the signal-to-noise ratio.

1. Reference data set from sine sweep excitations

An amplitude variation on the multisine excitation input was performed using the forward wing outboard control surfaces. The frequency response estimates are examined relative to a reference estimate produced using sine sweep data sets. Frequency response estimates using each of four sine sweep excitations were generated, and their Gaussian distribution parameters estimated. Figure 15 shows the mean frequency response estimate using the sine sweep data, as well as the ranges of the estimate employing +/- 3 standard deviations. The sine sweep data sets were generated with control surface deflection amplitudes of 4°. The standard deviation plots can also be interpreted as confidence intervals on the mean. The confidence interval indicates how much uncertainty there is in the estimate of the true mean.

An interval estimate on upper and lower bounds on the mean give numerical information for the parameter and also indicate the level of confidence that can be placed on the numerical value based on the samples. The confidence interval on the mean value can be computed using the normal distribution function. Upper and lower limits of an interval are defined such that, with a specified level of confidence, the true parameter will lie in this interval. The interval (LB,UB) is the 100(1-α)% confidence interval for a parameter Θ,[14] as expressed in Equation 11. The probability that the parameter lies between the bound's values is (1-α).

$$P(LB < \Theta < UB) = 1 - \alpha \qquad \text{Equation 11}$$

Estimating the confidence interval for the mean of a normal distribution with an unknown variance uses Student's t-distribution and the sample variance in computing the confidence interval. The uncertainty on the mean is computed by transforming the process to a standardized random variable, assuming the maximum likelihood

estimator for the mean is itself normal, and the probability density function of a Gaussian process[14]. This results in the uncertainty on the mean as expressed in the following equation

$$[LB, UB] = \mu \pm \frac{t_{(\alpha/2,Ns-1)}\,\bar{\sigma}}{\sqrt{Ns}} = \mu \pm c\sigma \qquad \text{Equation 12}$$

Here, the number of experiments included, Ns, is 4. The standard deviation lines in the figure correspond to a confidence levels 99.5%.

2. Amplitude variation

The amplitude of the multisine excitation was increased from 0.25 up to 2.5. This is not a measure of the maximum control surface deflection, but rather the multiplier for the multisine time history. Calculation of the multisine signal amplitude has been described in a previous section of this paper.

The frequency response estimates produced by each of the excitation amplitudes is shown in Figure 15. The lower amplitude results show more scatter than the higher amplitude results. As the amplitude increases, the results also tend to agree more closely with the sine sweep results. This trend is illustrated more explicitly in Figure 15Figure 16. The multisine data sets are plotted as a function of the excitation amplitude. The frequency response estimates for each multisine data set are shown as deviations from the reference data set. From Figure 16, it is evident that the agreement between the reference data set and the multisine data improves with increased excitation amplitude.

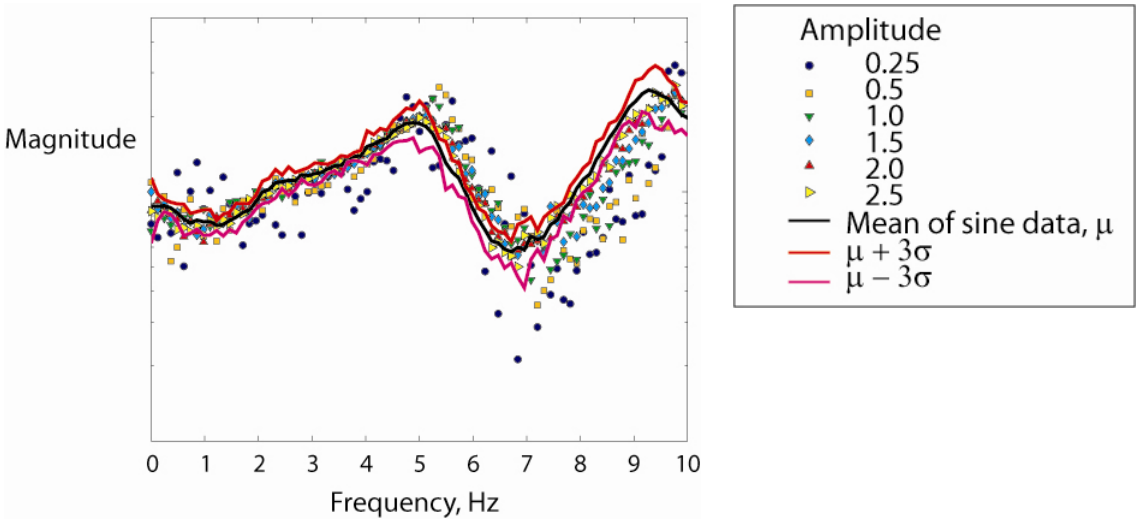

Figure 15. Amplitude variation of multisine signal to forward wing outboard surfaces

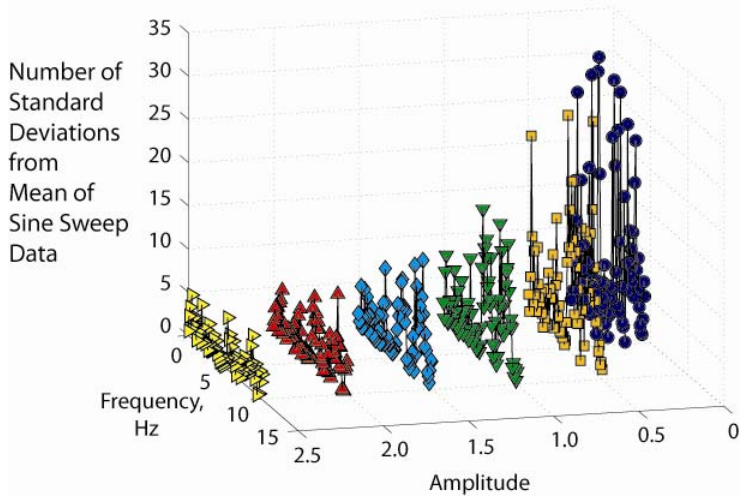

Figure 16. Deviation relative to sine sweep reference data; effect of multisine signal amplitude

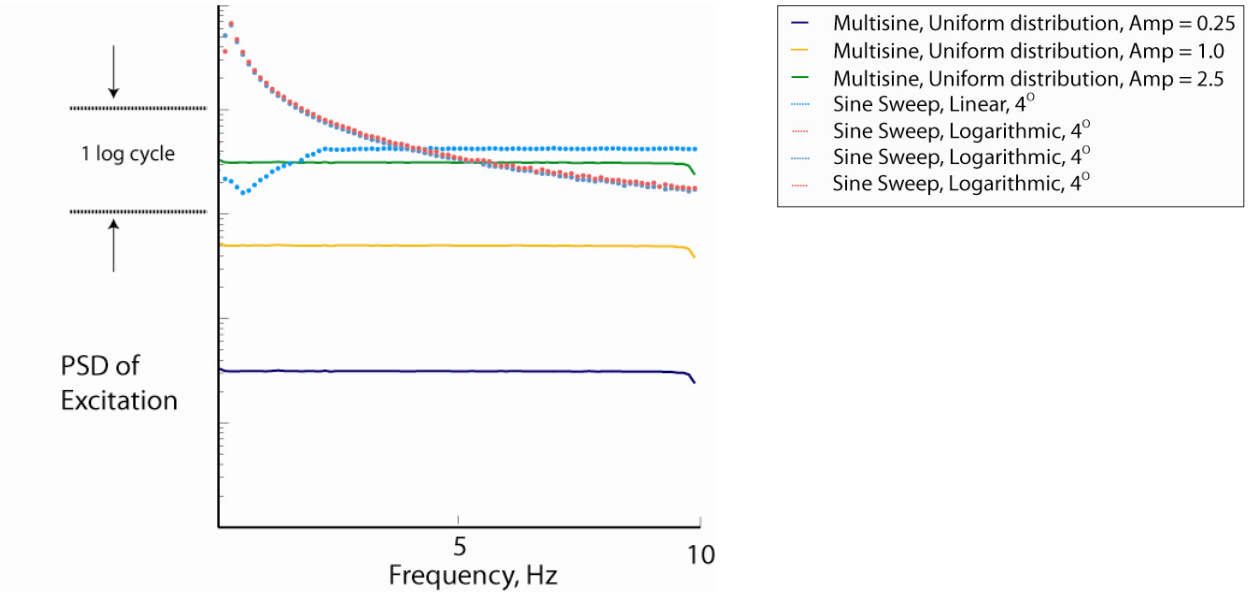

Figure 17. Power spectral density of excitation signals

Power spectral density functions of the excitation signals were computed; the resulting data is shown in Figure 17. The first three lines (blue, orange, green) show the results from analysis of multisine signals which were sent to the forward wing outboard surface. Each of these signals contained frequency content from 0.1 to 10 Hz. Each plot shows the flat response over this frequency range, followed by a steep drop at 10 Hz. The three curves are for three amplitudes shown in the previous data reduction, 0.25, 1.0 and 2.5. The PSD magnitudes increase as the square of the excitation amplitudes.

The input power in the frequency range of interest is flat, without any significant amount of variation. These results were produced with Fourier analysis block size of 4096 points with 95% overlap and rectangular windowing. Significant variation of the PSD in the range of signal frequency content would have been a symptom indicating that differences could be due to poor choice of Fourier analysis frequency spacing, as discussed earlier in this paper.

Figure 17 also shows the PSDs of the four sine sweep data sets which were analyzed to provide the reference frequency response estimate in the previous discussion. Three of these sweeps are logarithmic and one is linear from 2 to 18 Hz. In all cases, the amplitude of the excitation was such that the control surfaces oscillated ±4°.

Amplitude is defined differently for the different types of sweeps; the power spectral density provides better comparison of the relative power applied at a given frequency for the different methods. When the amplitude of the multisine data is 2.5, the input power near the first aeroelastic mode is close to the input power of the logarithmic sine sweeps and slightly below the linear sine sweep. The lower amplitude multisine signals have significantly less input power. Less input power means that the turbulence in the wind tunnel will be a relatively larger component of the model excitation, and that the overall dynamic response will be reduced. Both of these considerations reduce effective signal-to-noise ratio, resulting in a noisier and less accurate frequency response estimate.

The signal-to-noise ratio may be responsible for some of the differences observed between the single control pair input data using sine sweeps and using multisine excitations. Although the differences are qualitatively small, and may be within the accuracy of the methods employed, this is one issue which deserves continued investigation and quantification.

C. Excitation method effects & simultaneous actuation effects

In the previous comparisons of sine sweep and multisine responses, the assessment that the frequency responses were qualitatively similar was offered. The type of excitations (sine sweep or multisine) appears to produce more variation in the frequency response estimates than the simultaneous multisine excitation produces relative to the single surface multisine excitation results. The root causes of these differences have not been identified. The following comparisons are presented to illustrate the range of the variations, the repeatability and statistical quantification of the variation due to each of the sources- excitation type and simultaneous actuation.

1. Qualitative comparison

Several data sets were obtained exciting the model using only the forward wing outboard surface pair for the trimmed flight configuration. The resulting frequency response estimate magnitudes from 4 sine sweep data sets, 5 uniform distribution multisine data sets, 4 specific frequency sine dwells, and 4 tailored multisines are shown in Figure 18. The sine sweep data and the multisine data form distinctive sets, particularly separable between the peaks of the first and second aeroelastic modes, which have frequencies of approximately 5 Hz and 9.5 Hz respectively. The sine dwell data corresponds well with the sine sweep data points. The uniquely tailored multisine data, containing specific frequencies and analyzed at those specific frequencies agrees better with the sine sweep data, except at the valley near 6.7 Hz.

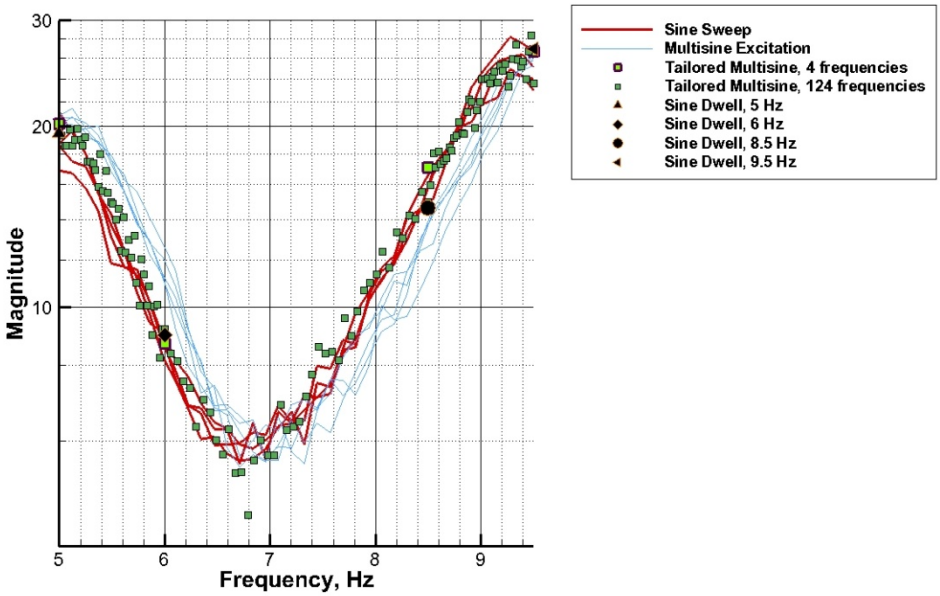

Figure 18. Magnitude of SGFWO/FWO; Closed loop trimmed configuration

The amplitudes of the signals are defined differently for the sine sweeps and the multisine excitations, and overall signal power has been shown to be a cause of variation. Power spectral density analysis of each of the command signals, Figure 19, refutes the idea that more energy is put into the system by the sine sweeps than by the multisine excitations. The figure shows an example of the energy input; no formal statistical analysis was performed to assess the significance of this factor. Over the frequency range of consideration, these sweeps are as closely matched in input energy as possible. The tailored multisine signal has more power over this frequency range, but does not appear to identify the system more cleanly than the other data sets. This conclusion is based on the perceived scatter of tailored multisine data set, shown by the green squares shown in Figure 18.

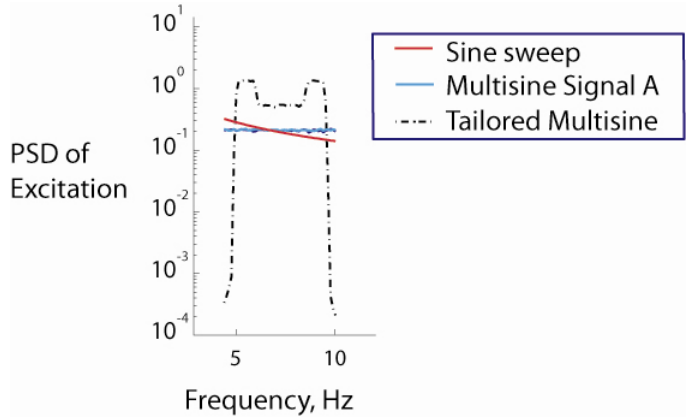

Figure 19. Power spectral density of command to forward wing outboard control surfaces

2. Quantitative analysis

Qualitative statements have been made describing the differences among the data sets analyzed. It is desired to determine if the differences among the data sets are significant, and to what underlying factors these differences may be attributable. Specifically, for this investigation, it is desired to determine if applying the multisine signals simultaneously produces a significant difference relative to when each surface pair is actuated individually.

Statistical methods were applied to a subset of the frequency response estimate results to evaluate the significance of simultaneous excitation and also excitation type. In the comparisons of the data sets, variations among these sets are observed. Analysis of variance (ANOVA)[15] was performed on frequency response estimates of the strain gauge forward wing outboard response due to forward wing outboard surface deflections.

The ANOVA utilized in this study employs the statistical f-test to determine where there exists a significant difference among the mean values of two data treatments, or levels of a factor. A fixed effects model is used here, i.e., predetermined values of the factor are used. The variance between groupings of the data, separated by their factor values, is compared with the variance of the entire data set.

The null hypothesis assumes that there is no difference among the levels for a factor. A test statistic is computed for each factor. If the null hypothesis is accepted, there is an implication that no relation exists between the factor levels and the response. Critical values associated with significant level, a, are compared to the calculated test statistic. When the test statistic exceeds the critical value, the null hypothesis is rejected with $(1-\alpha)*100\%$ confidence. A value of $\alpha = 0.05$ implies that the null hypothesis is rejected 5% of the time when it is in fact true; the factor is considered significant with 5% confidence. Whether a factor is deemed significant is a subjective evaluation, as the significance level has to be chosen. Standard practice in many fields is to use a significance level of $\alpha = 0.05$.

From each frequency response estimate, the magnitude was extracted at four distinct frequencies, where sine dwell data had also been acquired: nominally 5, 6, 8.5 and 9.5 Hz. These frequencies were chosen to span the range of the first and second aeroelastic modes, and include the regions where the frequency responses exhibit the largest amount of variation. There were 42 experimental data sets available for comparison: 1 sine dwell; 4 sine sweeps; 7 uniform power multisines sent only to the FWO pair; 4 tailored power multisine signals, sent only to the FWO pair; and 26 orthogonal multisine sets sent to all surfaces simultaneously. One of the orthogonal multisines did not have frequency content above 6 Hz, so for the higher frequency comparisons, only 41data sets were available. The magnitudes of each of these data sets are shown at the extracted frequencies in Figure 20. There are two data sets shown near 8.5 Hz because the Fourier analysis frequencies were nearly equally spaced relative to the sine dwell excitation frequency. The exact analysis frequencies where the frequency response estimate data was extracted were 5.005, 5.981, 8.423, 8.545, and 9.521 Hz.

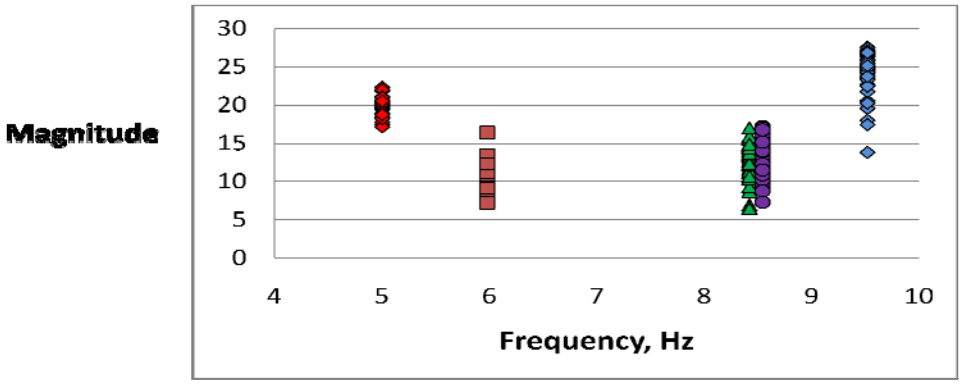

Figure 20. ANOVA data sets

At each frequency, two separate single-factor ANOVA analyses were performed. The first analysis grouped the data by excitation type: sinusoidal excitation and multisine excitation. Examples of this grouping are shown in Figure 21 for 5 Hz and 9.5 Hz data sets.

The second ANOVA analysis utilized only the multisine excitation data, grouped by number of simultaneous multisine excitations: single control surface pair and all 6 control surface pairs. Examples of this grouping are shown in Figure 21 for 5 Hz and 9.5 Hz data sets.

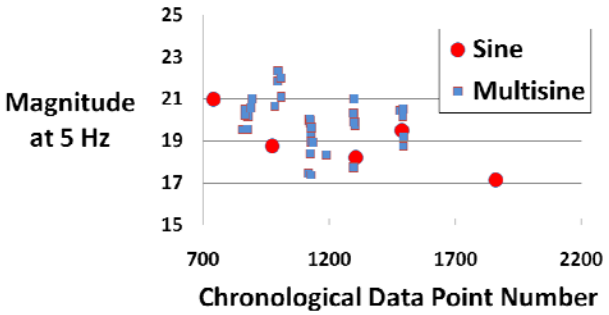

a) 5 Hz

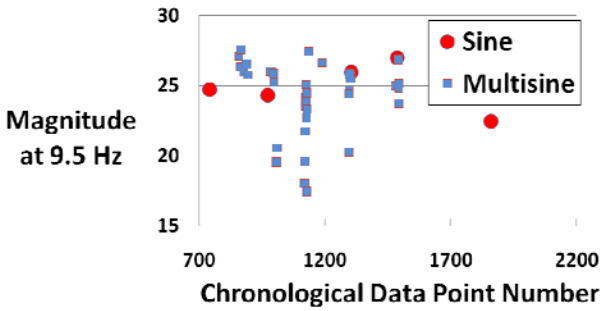

b) 9.5 Hz

Figure 21. ANOVA data sets, sorted by excitation type

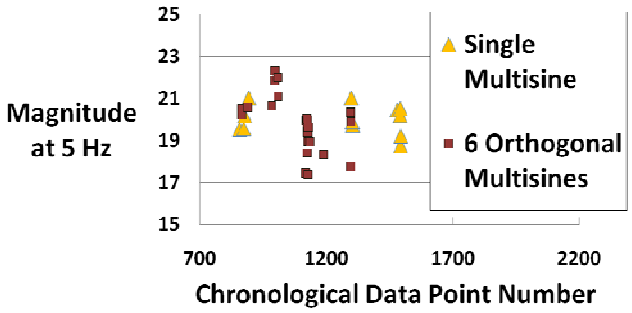

a) 5 Hz

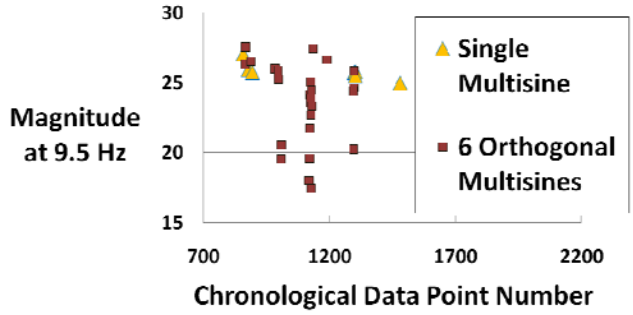

b) 9.5 Hz

Figure 22. ANOVA data sets, sorted by number of simultaneously applied multisine excitation signals

Table 1. Percent confidence, (1-α)*100%, that the specified factor is significant; One-way ANOVA results (* denotes resu1ts with 1 outlier point removed; small excitation amplitude physical cause of outlier)

Factor Name:	Excitation Type	Simultaneous Multisine
Factor Levels:	(Sine ; Multisine)	(1 signal ; 6 signals)
Frequency (Hz)		
5.005	92	32
5.891	98	24
8.42	97	49
8.54	99	73
9.521	48	94
9.521*	40	94

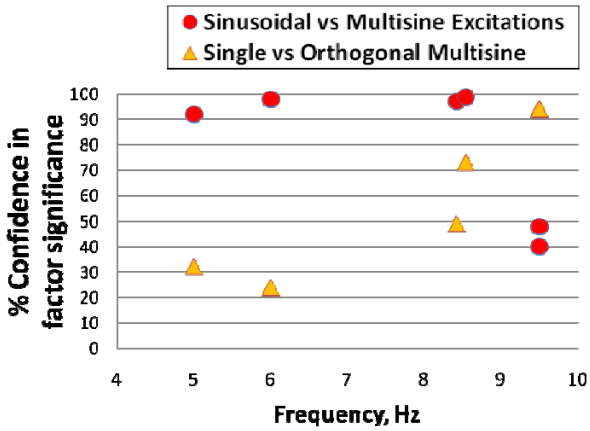

Figure 23. Percent confidence, (1-α)*100%, that the specified factor is significant; One-way ANOVA results

The ANOVA results, Figure 23, are the most dramatic at frequencies on the downslope of the first aeroelastic mode, i.e., 6 Hz. At 6 Hz, the ANOVA results with $\alpha = 0.02$ show that the responses due to sine and multisine excitation are not drawn from the same underlying process; the ANOVA states that they are drawn from processes that have different mean values. They indicate this with 98% confidence, (1-α)*100%. Differences in the underlying process are statistically related to the observed differences between the two data sets, rather than being attributable to random error.

Performing ANOVA using the single and orthogonal multisine excitations, the results show that the responses are drawn from processes which have the same mean. In this case, this can only be asserted with 76% confidence. On the graph in Figure 23, this is indicated by the data at 6 Hz, and 24% confidence. The confidence with which is it asserted that the factor is not significant is (100-24) %, or 76%. Random error accounts for the differences observed between these data sets, rather than underlying process differences.

Summarizing the results across all of the frequencies, the ANOVA results show that the excitation type- sine sweep or multisine- is a significant source of variation in the response with greater than 90% confidence for all frequencies except 9.5 Hz. The results also show that simultaneous application of the multisine signals is not a likely source of variation of the response, again excepting the information at 9.5 Hz.

V. Discussion

A. Sources of error

Assuming that the dynamic system is linear is fundamental to the excitation and data analysis method applied in this work. It is assumed that exciting the system at a specified frequency generates response only at that frequency. Nonlinearities in the system can produce responses at frequencies other than those present in a particular excitation. In simultaneous multisine excitation, this can have the effect of the response created by one control surface excitation being attributed to a different control surface excitation. The JWS data does not appear to have significant nonlinearities in the frequency range investigated, shown by the agreement between the multisine excitation responses with a single control surface pair active and those responses due to all surfaces simultaneously actuated with the orthogonal multisine excitation sets.

A potential source of error is the physical interference among multiple control surfaces. In an aeroelastic system, interference effects can be aerodynamic, structural or a combination. Control surfaces in close proximity to each other will affect the flow field that each sees. The local hinge moments can also influence the structural states of each other. These effects can also be dependent on the relative phasing of the control surfaces. Interference effects are often ignored in determining control surface frequency responses and control surface authority. In systems where the interference is significant, multiple experimental data sets are required to identify these effects, rather than reliance on a single data set acquired using the described simultaneous excitation data.

B. Advantages / disadvantages of multisine excitations

The primary advantage of using multisine excitations is that a large number of control effectors can be assessed simultaneously. For a system such as the JWS, this greatly reduces the test time. Multisine excitations also offer time savings in that the frequency content for all modes is present from the beginning of the excitation. This

situation is in contrast to sine sweeps, which generally progress up or down in frequency over time. System identification for an aeroelastic system requires excitation through the modal frequency range, which often pushes the model beyond a limit when they are encountered. When a limit is encountered, the excitation is halted, the amplitude reduced and the excitation restarted from the beginning. This process of rescaling the excitation can be cumbersome and time consuming. For a sine sweep, a limit may be encountered after some time spent exciting the system at lower frequencies, whereas a multisine excitation with too much amplitude generally puts the system beyond its limit from the outset, so a quick test burst of excitation suffices to verify that the scaling is acceptable.

Simultaneous excitation also offers the advantage that a single data set can contain all data required for open loop system extraction using a closed loop system. One-at-a-time excitation requires that the user organize the data into proper positions within the return difference matrix. Simultaneous actuation removes these data organizational tasks which can be prone to human error.

Multisine signals avoid a problem inherent with the sine sweeps; multisine signals do not excite the system with a single frequency. While excitation at the modal frequencies is desirable from a response standpoint, from a test perspective it often causes the model to exceed structural or travel limits. In the case of a free-flying vehicle or model, at low frequencies, multisine excitation avoids this problem.

There are also some potential drawbacks to employing a multisine excitation. The biggest drawback is that visual information is not able to be interpreted in real time by a test engineer. Using sine sweeps produces amplified motion and amplified sensor responses as the frequencies corresponding to the aeroelastic modes are excited. Direct observation as the data is acquired is often sufficient for determining if the data acquired will be usable for system identification data. It may be a matter of test engineer acclimatization in the case of the latter issue.

C. Future work and open questions

The JWS model provided a testbed for obtaining a great deal of data using a large number of control surfaces. The shortcoming in this data set is the lack of open loop and closed loop data corresponding to a single test state. Additional work is being performed using multisine excitation data obtained from wind tunnel testing of the SemiSpan SuperSonic Transport (S4T)[16,17] to address issues pertinent to open loop system extraction. Further work is also required to identify the sources of deviations in the data sets, and to quantify the uncertainties due to these sources.

Turbulence is a source of uncertainty or error present in system identification work, regardless of the excitation type. The influence of turbulence on the identified system responses is being investigated further using S4T experimental and simulation data.

ANOVA results showed that the excitation type- sine sweep or multisine- was a more significant source of variation in the response than utilizing simultaneous orthogonal multisines. The root cause of the response variation with excitation type has not been identified- it is possibly physical or possibly related to data processing methods. This is being further investigated using S4T data.

D. Lessons learned

It is essential to evaluate the signal-to-noise ratio. This evaluation is best accomplished by acquiring a sample data set and computing the quantities of interest in near real time. Increasing the overall amplitude to improve signal to noise ratio should take precedence over using the exact multisine signal set generated. Regenerating orthogonal sets may reduce the peak value of the time histories, or if there are only a few time points that exceed limits, these peaks can be shaved off, with a much less significant effect than insufficient overall signal power.

The frequencies of the Fourier domain analysis are not required to agree with the excitation frequencies. In performing discrete time Fourier analysis, the frequency range is divided into discrete frequency bins. The multisine signals have frequency content at discrete, spaced frequencies. It is sufficient for each of the Fourier domain analysis bins to have excitation from each signal within the bin's frequency range. Effects of analyzing the data using frequencies which are too finely spaced are observed as bi-modal or scattered (seemingly noisy) power spectral density functions.

The generated multisine signals have content at specific frequencies, however, implementation issues slightly modified the frequency content of the recorded signals. These implementation issues degraded the Fourier domain analysis results and required overlap averaging to compensate. Miniscule lags in data acquisition change the precise frequencies that are measured; this error can produce large inaccuracies if exact frequency matching is performed without a sufficient number of data averages employed.

VI. Conclusion

Applying this implementation of orthogonal multisine excitations to an aeroservoelastic problem with a large number of control effectors offers much promise for reducing test time required for system identification. Statistical analysis demonstrates the equivalence of simultaneous orthogonal multisine excitations and individual multisine excitations. Design of the multisine excitation sets should be performed with the specific system dynamics in mind, and with the data analysis requirements firmly understood. There are open questions regarding small variations produced by using a multisine signal or a sine sweep which are being investigated through additional experimental data and simulation.

References

[1] Morelli, E.A. "Flight-test experiment design for characterizing stability and control of hypersonic vehicles," *Journal of Guidance, Control, and Dynamics*, Vol. 32, No. 3, May-June 2009, pp. 949-959.

[2] Martinez, J., "An overview of SensorCraft capabilities and key enabling technologies," 26th AIAA Applied Aerodynamics Conference, No. AIAA-2008-7185, Honolulu, Hawaii, August 2008.

[3] Reichenbach, E., "Aeroservoelastic design and test validation of Joined Wing SensorCraft," 26th AIAA Applied Aerodynamics Conference, No. AIAA-2008-7189, Honolulu, Hawaii, August, 2008.

[4] LeDoux, S., Vassberg, J., and Fatta, G., "Aerodynamic cruise design of a Joined Wing SensorCraft," 26th AIAA Applied Aerodynamics conference, No. AIAA-2008-7190, Honolulu, Hawaii, August 2008.

[5] Scott, M., "SensorCraft free-flying aeroservoelastic model design and fabrication," 52nd AIAA/ASME/ASCEAHS/ASC Structures, Structural Dynamics and Materials Conference, Denver Colorado, April 2011.

[6] Sharma, V., and Reichenbach, E.," Development of an innovative support system for SensorCraft Model," 52nd AIAA/ASME/ASCEAHS/ASC Structures, Structural Dynamics and Materials Conference, Denver Colorado, April 2011.

[7] Reichenbach, E., and Sexton, B., "Joined-Wing SensorCraft aeroservoelastic wind tunnel test program," 52nd AIAA/ASME/ASCEAHS/ASC Structures, Structural Dynamics and Materials Conference, Denver Colorado, April 2011.

[8] Scott, Robert C., Castelluccio, Mark A., Coulson, David A., and Heeg, Jennifer, "Aeroservoelastic wind-tunnel tests of a free-flying, Joined-Wing SensorCraft model for gust load alleviation," 52nd AIAA/ASME/ASCEAHS/ASC Structures, Structural Dynamics and Materials Conference, Denver Colorado, April 2011.

[9] Staff of the Aeroelasticity Branch, "The Langley Transonic Dynamics tunnel," Langley Working Paper LWP-799, Sept 1969.

[10] Hardin, Jay C., Introduction to time series analysis, NASA Reference Publication 1145, Nov 1990.

[11] Pototzky, Anthony S., Wieseman, Carol D., Hoadley, Sherwood T., and Mukhopadhyay, Vivek, "Development and testing of methodology for evaluating the performance of multi-input/multi-output digital control systems," NASA TM-102704, Aug 1990.

[12] Pototzky, Anthony S., Wieseman, Carol D., Hoadley, Sherwood T., and Mukhopadhyay, Vivek, "On-line performance evaluation of multiloop digital control systems," Journal of Guidance, Control and Dynamics, 1992, Vol 15, No. 4.

[13] Oppenheim, Alan V. and Schafer, Ronald W., Discrete-time signal processing, 1989, Prentice-Hall, Inc, Englewood Cliffs, New Jersey.

[14] Soong, T.T, "Probabilistic modeling and analysis in science and engineering," John Wiley & Sons, New York, 1981.

[15] Anonymous, *NIST/SEMATECH e-handbook of sStatistical methods*, URL: http://www.itl.nist.gov/div898/handbook/ppc/section2/ppc231.htm [cited Feb 6, 2011].

[16] Perry, Boyd, et al., "Plans and status of wind-tunnel testing employing an aeroservoelastic aemispan model," 48th AIAA/ASME/ASCEAHS/ASC Structures, Structural Dynamics and Materials Conference, No. AIAA-2007-1770, Honolulu, Hawaii, April 2007.

[17] Christhilf, David, Pototzky, Anthony S., and Stevens, William, "Incorporation of SemiSpan SuperSonic Transport (S4T) aeroservoelastic models into SAREC-ASV simulation", AIAA Modeling and Simulation Technologies conference, AIAA-2010-8099, Toronto, Ontario, August 2010.